Imaging Agents

Deutsche Ausgabe: DOI: 10.1002/ange.201503417
Internationale Ausgabe: DOI: 10.1002/anie.201503417

Synthesis and Evaluation of Gd^{III}-Based Magnetic Resonance Contrast Agents for Molecular Imaging of Prostate-Specific Membrane Antigen**

Sangeeta Ray Banerjee, Ethel J. Ngen, Matthew W. Rotz, Samata Kakkad, Ala Lisok, Richard Pracitto, Mrudula Pullambhatla, Zhengping Chen, Tariq Shah, Dmitri Artemov, Thomas J. Meade, Zaver M. Bhujwalla, and Martin G. Pomper*

Abstract: *Magnetic resonance (MR) imaging is advantageous because it concurrently provides anatomic, functional, and molecular information. MR molecular imaging can combine the high spatial resolution of this established clinical modality with molecular profiling in vivo. However, as a result of the intrinsically low sensitivity of MR imaging, high local concentrations of biological targets are required to generate discernable MR contrast. We hypothesize that the prostate-specific membrane antigen (PSMA), an attractive target for imaging and therapy of prostate cancer, could serve as a suitable biomarker for MR-based molecular imaging. We have synthesized three new high-affinity, low-molecular-weight Gd^{III}-based PSMA-targeted contrast agents containing one to three Gd^{III} chelates per molecule. We evaluated the relaxometric properties of these agents in solution, in prostate cancer cells, and in an in vivo experimental model to demonstrate the feasibility of PSMA-based MR molecular imaging.*

Magnetic resonance (MR) imaging is a clinically relevant, noninvasive diagnostic tool for high-resolution anatomic and functional imaging. Molecular MR imaging enables the visualization of biological markers in vivo.[1] Gd^{III}-based contrast agents are widely accepted by clinicians because they are easy to administer and provide T_1-weighted, positive contrast. Although progress has been made in the design of contrast agents with high relaxivity, sensitivity remains a limiting factor for molecular MR imaging. For use in molecular imaging applications (specifically, for imaging receptor or protein expression), Gd^{III}-based contrast agents seldom exceed the limit of detection.[1b,c,2] With signal amplification strategies, MR might offer a sensitive modality for molecular imaging complementary to radionuclide-based techniques.[3] Although amplification strategies could improve the sensitivity of a targeted agent, shifting from a simple, low-molecular-weight compound to a larger, multiplexed entity may significantly alter the pharmacokinetic profile of the agent.[1b,c,2a] Combining a receptor-specific high-affinity ligand with multimeric Gd^{III} agents for detection has been described as one solution for enabling MR-based receptor imaging.[4b,5] Sherry et al. have addressed these issues by generating contrast agents with very high binding affinities (K_d) such that the amount of agent needed for detection by MR could be minimized.[4] An example of that approach includes molecular imaging of VEGFR2 (vascular endothelial growth factor receptor 2) by preparing a multimeric Gd dendron with high longitudinal relaxivity (r_1) values.[4b] Additionally, other multimeric agents with r_1 values optimized for higher field strengths have been reported because MR imaging, both experimental and clinical, are moving to higher fields.[6] Optimizing relaxivity at high field provides the advantages of greater signal-to-noise and contrast-to-noise ratios (SNR/CNR) and the additional benefits of higher spatial resolution and reduced acquisition times. Combination of these concepts, namely the use of high-affinity targeting moieties with sensitive multimeric contrast agents, provides the rationale to investigate targeted MR imaging of cells and tissues expressing the prostate-specific membrane antigen (PSMA).

PSMA is overexpressed in primary and metastatic prostate cancer, particularly with respect to the castration-resistant form.[7] Furthermore, PSMA is expressed by most solid tumors and tumor neovasculature.[8] Imaging PSMA can provide insight into androgen signaling[9] and cell response to taxane therapy.[10] We and others have developed a variety of imaging agents for PSMA that employ optical, nuclear, and MR imaging.[11] For the attachment of large molecular fragments such as radiometal complexes (^{99m}Tc, ^{68}Ga, ^{111}In)[11a,c] to nanoparticles[11d,12] we devised a tripartite strategy containing a PSMA-targeting moiety, a linker for pharmacokinetic tuning, and a chelating agent. We hypothesized that PSMA would be a suitable biomarker for MR molecular imaging because of the extracellular location of the ligand binding site and the estimated high receptor concentration per cell (circa 3.2 μM/cell volume; see the Supporting Information). To test the hypothesis, we synthesized three

[*] Dr. S. R. Banerjee, Dr. E. J. Ngen, Dr. S. Kakkad, A. Lisok, R. Pracitto, M. Pullambhatla, Dr. Z. Chen, Dr. T. Shah, Dr. D. Artemov, Dr. Z. M. Bhujwalla, Dr. M. G. Pomper
The Russell H. Morgan Department of Radiology and Radiological Science, Johns Hopkins University
Baltimore, MD 21231 (USA)
E-mail: sray9@jhmi.edu
M. W. Rotz, Dr. T. J. Meade
Chemistry, Northwestern University
Evanston, IL 60208 (USA)

[**] We would like to thank A. Jacobs, D. Jacob, G. Green, Dr. B. Wang, Dr. M. F. Penet, V. S. Harrison, and Dr. K. W. Macrenaris for initial assistance with the experiments. Funding for the project was provided by the NIH CA148901 (to S.R.B.), CA151838, CA134675 (to M.G.P.).

Supporting information for this article is available on the WWW under http://dx.doi.org/10.1002/anie.201503417.

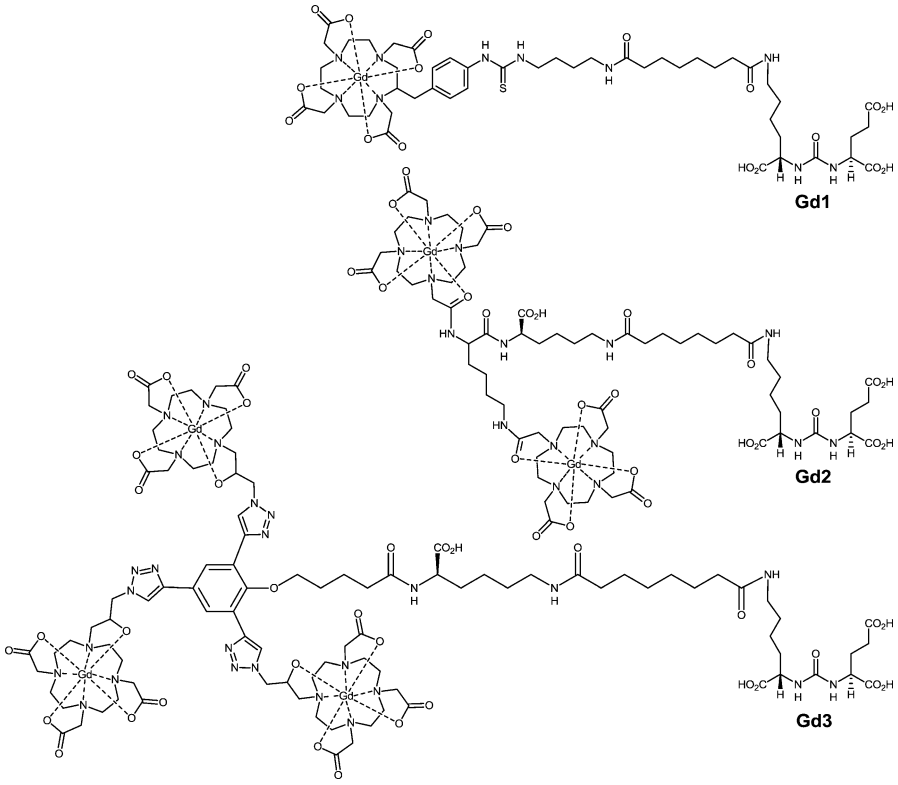

Figure 1. Structures of PSMA-targeted MR contrast agents Gd1–Gd3.

PSMA-targeted agents bearing one, two, or three Gd^{III} complexes, Gd1, Gd2 and Gd3, respectively (Figure 1). We then evaluated the PSMA binding affinities and relaxivities of the synthesized agents. Cellular uptake of the agents in PSMA-expressing cells and isogenic non-expressing control cells was evaluated using inductively coupled plasma mass spectrometry (ICP-MS). Finally, the ability of the agents to distinguish PSMA-expressing cells from control cells was evaluated both in vitro and in vivo by MR imaging.

Multistep solution-phase synthetic methods were developed to prepare the contrast agents and are outlined in Schemes S1–S3 in the Supporting Information. Lys–Glu urea was used as the targeting moiety for PSMA. To that targeting group were added varying numbers of the core macrocyclic chelating agent 1,4,7,10-tetraazacyclododecane-1,4,7-triacetic acid (DO3A) or 1,4,7,10-tetraazacyclododecane-1,4,7,10-tetraacetic acid (DOTA).[13] Gd1 contains a *p*-isothiocyanatobenzyl DOTA (DOTA-Bn-SCN) chelating agent. The structure of Gd1 is based on our recently reported lead ^{86}Y-labeled imaging agent for positron emission tomography (PET), which demonstrated high and specific tumor accumulation in a preclinical model.[11f] Gd2 was prepared by conjugation of the α- and η-amines of lysine with DO3A-NHS, employing a solution-based peptide synthesis strategy. Under the same conditions, yields of the coupling reactions were significantly improved when the reaction was performed in a sonication bath at room temperature. Gd3 contains a phenolic core to which three Gd^{III}-DOTA chelators were bound through rigid triazole linkages, as previously reported by Mastarone et al.[6b] using click chemistry. To that core was conjugated the PSMA-targeting functionality through the phenolic oxygen. The agents were purified by reverse-phase high performance liquid chromatography (HPLC) and were characterized by mass spectrometry. To ascertain any potentially negative effects of the Gd^{III}-containing portion of the agents on the binding affinities of the probes, values of the PSMA inhibition constant (K_i) for the agents Gd1, Gd2, and Gd3 were determined and are listed in Table 1.[11c] The known, high-affinity PSMA inhibitor *N*-{[((*S*)-1-carboxy-3-methylbutyl)-amino]carbonyl}-L-glutamic acid (ZJ43)[14] was used as a reference ligand. All agents retained high binding affinity, with K_i values in the low nanomolar range (Gd1 > Gd3 > Gd2). When imaged at 9.4 T and 25 °C, solution phantoms indicated r_1 relaxivities in phosphate-buffered saline (PBS) that varied between 3.0 and 6.2 $mM^{-1}s^{-1}$ per Gd^{III} and between 3.0 and 12.5 $mM^{-1}s^{-1}$ per contrast agent (Table 1). Unexpectedly, the r_1 value of Gd1 was slightly lower than that of the FDA-approved clinical contrast agents Dotarem or Prohance. Although the measured relaxivity for Gd2 seems surprisingly high, similar values have been reported at 9.4 T by Caravan et al.[6a] and by León-Rodríguez et al.[4b] Among the three compounds tested, Gd2 may have the optimum values for the inner-sphere water exchange rate, τ_m, and the rotational correlation time, τ_r, required for imaging at this field strength. The unexpected decrease in relaxivity of Gd3 compared to that reported by Mastarone et al.[6b] may be the result of the addition of a long PSMA-targeting construct to the bulky trimeric core, causing an incrementally longer τ_r value and a slight decrease in the r_1 relaxivity at 9.4 T. This effect could be exacerbated by measurement at 25 °C rather than 37 °C, the temperature used by Mastarone et al.,[6b] because lower temperature would further slow molecular motion.[6a]

Table 1: Selected physical properties of contrast agents.

Compound	Molar Mass [g mol^{-1}]	r_1[a] [mM^{-1} s^{-1}]	K_i [nM][b]	95 % CI of K_i [nM]
Gd1	1250.40	3.0	0.45	0.36–0.55
Gd2	1803.13	6.2/12.5	18.18	14.07–22.16
Gd3	2651.03	3.3/9.81	7.19	5.17–10.01

[a] Relaxivities listed indicate the ionic/molecular relaxivity of the agents, respectively. [b] ZJ43 (K_i = 0.29; 95 % CI of K_i = 0.22–0.39 nM). CI = confidence interval.

To determine the specificity of Gd1–Gd3, we used isogenic PC3 human prostate cancer cells genetically modified to express high amounts of PSMA (PC3 PIP) and the corresponding wild-type, PSMA non-expressing cells

(PC3 flu;[11c] PIP and flu are names historically attached to PSMA + PC3 and PSMA− PC3 cells respectively, developed by Heston and co-workers[17]). After incubation with either Gd1 or Gd2, pelleted PC3 PIP (PSMA +) and PC3 flu (PSMA−) cells did not demonstrate any significant T_1-weighted MR contrast or changes in relaxation rate (R_1). Conversely, T_1-weighted images following incubation with Gd3, displayed significant MR contrast enhancement in PC3 PIP (PSMA +) cells compared to the unlabeled cells as well as to the PC3 flu (PSMA−) cells pellets (Figure 2). Cells

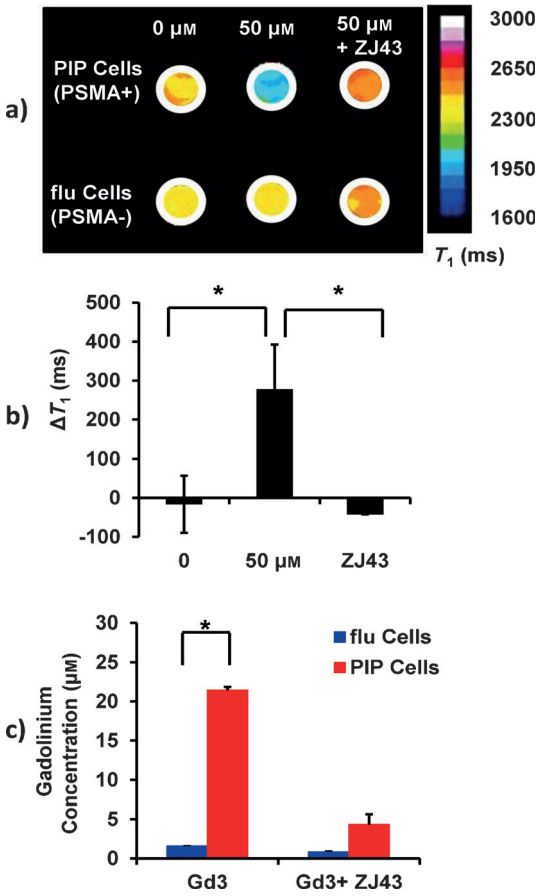

Figure 2. T_1 contrast enhancement generated by Gd3 in an isogenic human PC3 prostate cancer cell pair, PSMA+ PIP and PSMA− flu cells. a) Color-coded T_1 maps of PC3 PIP and PC3 flu cells. Relaxation rates were determined at 25 °C at 9.4 T. b) Quantification of ΔT_1 in PIP and flu cells ($n = 4$, $P < 0.05$) following treatment with Gd3. c) Cellular uptake of Gd3 in PC3 PIP and PC3 flu cells. The amount of Gd^{III} associated with PIP cell pellets was significantly higher than for the flu cell pellets. The accumulation of Gd3 in PIP cells was blocked by preincubating with ZJ43 ($n = 4$, $P < 0.05$).

incubated with Gd3 in the presence of ZJ43 showed only minor changes in T_1 value in both types of cells, indicated that ZJ43 was able to block the binding of Gd3 specifically. These results indicated that Gd3 exhibited receptor-specific cell binding on PC3 PIP (PSMA +) cells and displayed PSMA-mediated contrast enhancement.

The Gd^{III} cell uptake associated with the cell pellet images was analyzed by ICP-MS. The results indicated that there was negligible Gd^{III} associated with PC3 flu (PSMA−) cells for any of the agents whereas the PC3 PIP (PSMA +) cell pellets had an estimated intracellular Gd^{III} concentration of circa 22.8 μM for Gd3 followed by approximately 12.5 μM and 7.2 μM for Gd2 and Gd1, respectively (Figure 2c; Figure S1). A cell internalization assay revealed that the percent of incubated dose (% ID) that underwent internalization in PC3 PIP (PSMA +) cells for Gd1 and Gd2 was 9.06 ± 0.31 and 21.63 ± 3.51% after 4 h of incubation, respectively, whereas only 2.42 ± 0.11 and 3.51 ± 1.32% ID were associated with the cell surface at that time (Figure S2). Moreover, slightly higher nonspecific uptake was associated with Gd2 in PC3 flu (PSMA−) cells, which might be related to the lower binding affinity of this agent compared to Gd1. As a further check on cellular uptake and internalization, a dual-modality Gd monomeric contrast agent labeled with rhodamine Red-X was prepared to confirm the PSMA-mediated internalization of this class of contrast agents (Figure S3). Fluorescence imaging of the PC3 PIP (PSMA +) cells confirmed the presence of contrast agent on the cell surface and within the cytosol, with a substantial fraction concentrated near the cell nucleus. We anticipate that entrapped Gd^{III} might not contribute to signal enhancement due to the lack of water accessibility.[15] Gd3 showed notable but moderate enhancement at 9.4 T because of significantly higher cell-surface exposure compared to either Gd2 or Gd1.

A time-dependent internalization study was performed for Gd3 (Figure S4) after 1, 4, and 24 h of incubation. Intracellular uptake at 1 and 4 h was high and specific, 28.30 ± 0.47 and 39.92 ± 3.59% ID, respectively, in PC3 PIP (PSMA +) cells, whereas at 24 h post-incubation 89.69 ± 3.90% ID was detected. A similar amount of Gd (circa 33–37% ID) was associated with the cell membrane at those same time points. The results indicated that detectable T_1-weighted enhancement of Gd3 in PC3 PIP (PSMA +) cell pellets correlated well with the high, specific accumulation of Gd3 in PC3 PIP (PSMA +) cells.

To gain further insight into the pharmacokinetics of Gd1–Gd3 we employed a radioactive lanthanide related to Gd^{III} and synthesized a ^{177}Lu-labeled analogue of Gd1 as a radiotracer to measure the resultant uptake in relevant tissues over time (Figure S5). The biodistribution of the radiotracer indicated rapid renal clearance and robust uptake in PC3 PIP (PSMA +) tumors. We expect a similar pharmacokinetic profile, including rapid renal clearance, for Gd1–Gd3, although the injected doses of the MR agents would be higher. We also assayed the Gd^{III} content of Gd3 using ICP-MS in selected tissues at 48 h post-injection, as shown in Table S1. Results showed that there was significantly less Gd^{III} present in all organs relative to the PC3 PIP (PSMA +) tumor except for in the kidney, which routinely shows higher uptake as a result of a combination of renal clearance and the known expression of PSMA in proximal renal tubules.[16]

In vivo MR imaging of Gd3 was performed on mice bearing PC3 PIP (PSMA +) and PC3 flu (PSMA−) tumor xenografts implanted subcutaneously in the lower right and left flanks respectively, after a single bolus intravenous injection (0.06 mmol kg^{-1}). Figure 3a displays quantitative contrast enhancement mapping (ΔR_1) of 1 mm slices for both

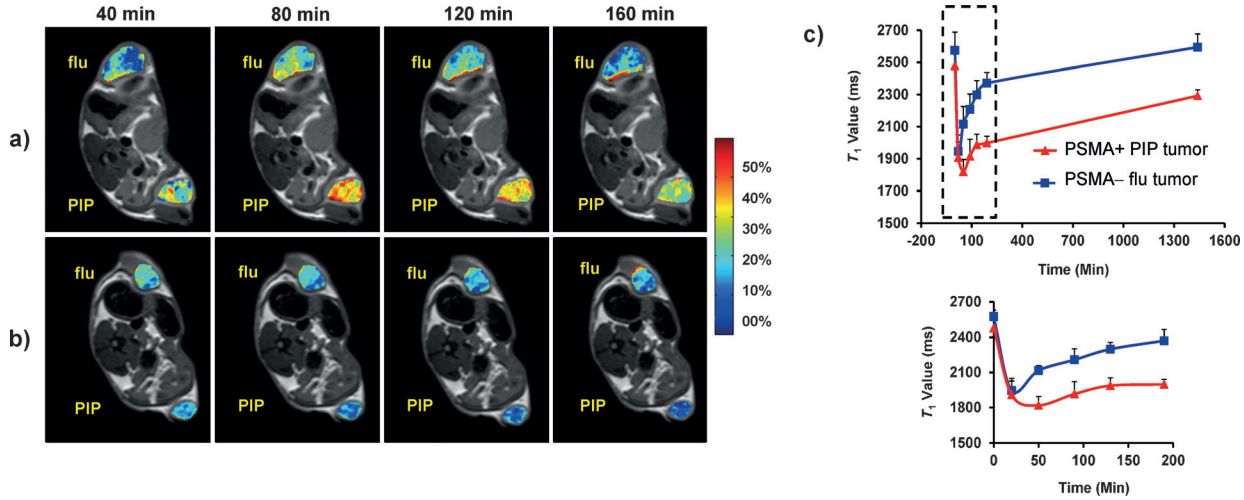

Figure 3. Gd3 MR imaging of human PC3 prostate cancer PIP (PSMA+) and flu (PSMA−) tumor xenografts in male NOD/SCID mice. a) Enhancement (ΔR_1%) maps in PC3 PIP (PSMA+) and PC3 flu (PSMA−) tumors are superimposed upon T_2-weighted images during 40-160 min after a single bolus injection of Gd3 into the tail vein. b) ΔR_1% maps in PSMA+ and PSMA− tumors of a trimeric Gd contrast agent without a PSMA-targeting moiety. c) T_1 time courses calculated for the entire volume of each tumor during 1–1600 min post injection (top). Enlarged region of the time course at 0–200 min (bottom).

tumors 40 to 160 min post-injection. Contrast enhancement remained constant for at least 3 h within the PC3 PIP (PSMA+) tumor, but it decreased quickly within the PC3 flu (PSMA−) tumor and muscle tissues. The T_1 values of the PC3 PIP (PSMA+) tumor (Figure 3c) reached a minimum of 1819 ± 76 ms (mean ± standard deviation, average 36% enhancement in R_1 values, $n = 4$) in the first 40 to 60 min, and remained constant at 29% until 90 min, and slowly decreased to 24% at 190 min after injection. For the PC3 flu (PSMA−) tumors, the highest contrast enhancement was approximately 24% at 20 min post injection, followed by a rapid decay in contrast enhancement ($\Delta R_1 < 20$% after 40 min). The results demonstrated specific contrast enhancement for PC3 PIP (PSMA+) tumors ($P \leq 0.05$) at 80 and 120 min post-injection. Figure 3b depicts results from other mice dosed in the same way but using a trimeric Gd probe without a targeting moiety, which showed no tumor enhancement.[6b] Additionally, an animal injected with a solution of PBS did not produce any change in the T_1 value (Figure S6).

By employing sensitive multimeric Gd^{III} complexes in combination with an established PSMA-targeting small molecule, PSMA-targeted MR molecular imaging was achieved in vitro and in vivo. Optimization of the constructs described for translational application in prostate and other cancers is under way.

Keywords: cancer · gadolinium · imaging agents · magnetic resonance imaging

How to cite: *Angew. Chem. Int. Ed.* **2015**, *54*, 10778–10782
Angew. Chem. **2015**, *127*, 10928–10932

[1] a) P. Caravan, *Acc. Chem. Res.* **2009**, *42*, 851–862; b) C. H. Huang, A. Tsourkas, *Curr. Top. Med. Chem.* **2013**, *13*, 411–421; c) G. M. Lanza, P. M. Winter, S. D. Caruthers, A. M. Morawski, A. H. Schmieder, K. C. Crowder, S. A. Wickline, *J. Nucl. Cardiol.* **2004**, *11*, 733–743; d) A. Pais, C. Gunanathan, R. Margalit, I. E. Biton, A. Yosepovich, D. Milstein, H. Degani, *Cancer Res.* **2011**, *71*, 7387–7397.

[2] a) D. Artemov, N. Mori, R. Ravi, Z. M. Bhujwalla, *Cancer Res.* **2003**, *63*, 2723–2727; b) S. D. Konda, M. Aref, S. Wang, M. Brechbiel, E. C. Wiener, *Magma* **2001**, *12*, 104–113; c) S. Aime, C. Cabella, S. Colombatto, S. Geninatti Crich, E. Gianolio, F. Maggioni, *J. Magn. Reson. Imaging* **2002**, *16*, 394–406.

[3] a) J. L. Major, T. J. Meade, *Acc. Chem. Res.* **2009**, *42*, 893–903; b) D. Artemov, *J. Cell. Biochem.* **2003**, *90*, 518–524.

[4] a) K. Hanaoka, A. J. Lubag, A. Castillo-Muzquiz, T. Kodadek, A. D. Sherry, *Magn. Reson. Imaging* **2008**, *26*, 608–617; b) L. M. De León-Rodríguez, A. Lubag, D. G. Udugamasooriya, B. Proneth, R. A. Brekken, X. Sun, T. Kodadek, A. D. Sherry, *J. Am. Chem. Soc.* **2010**, *132*, 12829–12831.

[5] X. Wu, S. M. Burden-Gulley, G. P. Yu, M. Tan, D. Lindner, S. M. Brady-Kalnay, Z. R. Lu, *Bioconjugate Chem.* **2012**, *23*, 1548–1556.

[6] a) P. Caravan, C. T. Farrar, L. Frullano, R. Uppal, *Contrast Media Mol. Imaging* **2009**, *4*, 89–100; b) D. J. Mastarone, V. S. Harrison, A. L. Eckermann, G. Parigi, C. Luchinat, T. J. Meade, *J. Am. Chem. Soc.* **2011**, *133*, 5329–5337.

[7] a) A. Ghosh, W. D. Heston, *J. Cell. Biochem.* **2004**, *91*, 528–539; b) M. I. Milowsky, D. M. Nanus, L. Kostakoglu, C. E. Sheehan, S. Vallabhajosula, S. J. Goldsmith, J. S. Ross, N. H. Bander, *J. Clin. Oncol.* **2007**, *25*, 540–547; c) W. C. Olson, W. D. Heston, A. K. Rajasekaran, *Rev. Recent Clin. Trials* **2007**, *2*, 182–190.

[8] M. C. Haffner, J. Laimer, A. Chaux, G. Schafer, P. Obrist, A. Brunner, I. E. Kronberger, K. Laimer, B. Gurel, J. B. Koller, C. Seifarth, B. Zelger, H. Klocker, M. Rasse, W. Doppler, N. H. Bander, *Mod. Pathol.* **2012**, *25*, 1079–1085.

[9] M. J. Evans, P. M. Smith-Jones, J. Wongvipat, V. Navarro, S. Kim, N. H. Bander, S. M. Larson, C. L. Sawyers, *Proc. Natl. Acad. Sci. USA* **2011**, *108*, 9578–9582.

[10] S. M. Hillier, A. M. Kern, K. P. Maresca, J. C. Marquis, W. C. Eckelman, J. L. Joyal, J. W. Babich, *J. Nucl. Med.* **2011**, *52*, 1087–1093.

[11] a) S. R. Banerjee, C. A. Foss, M. Castanares, R. C. Mease, Y. Byun, J. J. Fox, J. Hilton, S. E. Lupold, A. P. Kozikowski, M. G. Pomper, *J. Med. Chem.* **2008**, *51*, 4504–4517; b) S. R. Banerjee, M. Pullambhatla, Y. Byun, S. Nimmagadda, G. Green, J. J. Fox, A. Horti, R. C. Mease, M. G. Pomper, *J. Med. Chem.* **2010**, *53*,

5333 – 5341; c) S. R. Banerjee, M. Pullambhatla, Y. Byun, S. Nimmagadda, C. A. Foss, G. Green, J. J. Fox, S. E. Lupold, R. C. Mease, M. G. Pomper, *Angew. Chem. Int. Ed.* **2011**, *50*, 9167 – 9170; *Angew. Chem.* **2011**, *123*, 9333 – 9336; d) B. Behnam Azad, S. R. Banerjee, M. Pullambhatla, S. Lacerda, C. A. Foss, Y. Wang, R. Ivkov, M. G. Pomper, *Nanoscale* **2015**, *7*, 4432 – 4442; e) B. W. Tse, G. J. Cowin, C. Soekmadji, L. Jovanovic, R. S. Vasireddy, M. T. Ling, A. Khatri, T. Liu, B. Thierry, P. J. Russell, *Nanomedicine* **2015**, *10*, 375 – 386; f) S. R. Banerjee, C. A. Foss, M. Pullambhatla, Y. Wang, S. Srinivasan, R. F. Hobbs, K. E. Baidoo, M. Brechbiel, R. C. Mease, G. Sgouros, M. G. Pomper, *J. Nucl. Med.* **2015**, *56*, 628 – 634.

[12] a) S. S. Chandran, S. R. Banerjee, R. C. Mease, M. G. Pomper, S. R. Denmeade, *Cancer Biol. Ther.* **2008**, *7*, 974 – 982; b) Z. Chen, M. F. Penet, S. Nimmagadda, C. Li, S. R. Banerjee, P. T. Winnard, Jr., D. Artemov, K. Glunde, M. G. Pomper, Z. M. Bhujwalla, *ACS Nano* **2012**, *6*, 7752 – 7762.

[13] T. Frenzel, P. Lengsfeld, H. Schirmer, J. Hutter, H. J. Weinmann, *Invest. Radiol.* **2008**, *43*, 817 – 828.

[14] R. T. Olszewski, N. Bukhari, J. Zhou, A. P. Kozikowski, J. T. Wroblewski, S. Shamimi-Noori, B. Wroblewska, T. Bzdega, S. Vicini, F. B. Barton, J. H. Neale, *J. Neurochem.* **2004**, *89*, 876 – 885.

[15] a) E. Terreno, S. Geninatti Crich, S. Belfiore, L. Biancone, C. Cabella, G. Esposito, A. D. Manazza, S. Aime, *Magn. Reson. Med.* **2006**, *55*, 491 – 497; b) E. Di Gregorio, E. Gianolio, R. Stefania, G. Barutello, G. Digilio, S. Aime, *Anal. Chem.* **2013**, *85*, 5627 – 5631.

[16] D. A. Silver, I. Pellicer, W. R. Fair, W. D. Heston, C. Cordon-Cardo, *Clin. Cancer Res.* **1997**, *3*, 81 – 85.

[17] S. S. Chang, V. E. Reuter, W. D. W. Heston, N. H. Bander, L. S. Grauer, P. B. Gaudin, *Cancer Res.* **1999**, *59*, 3192 – 3198.

Received: April 15, 2015
Revised: May 26, 2015
Published online: July 23, 2015

